

Supporting Information

The metal dependence of single-metal mediated phosphodiester bond cleavage: a QM/MM study of a multifaceted human enzyme†

Rajwinder Kaur,^{a,‡} Mohamed M. Aboelnga,^{a,‡,§} Dylan J. Nikkel^a and Stacey D. Wetmore^{a,*}

^a *Department of Chemistry and Biochemistry, University of Lethbridge, 4401 University Drive West, Lethbridge, Alberta, Canada T1K 3M4.*

[§] *Present address: Chemistry Department, Faculty of Science, Damietta University, New Damietta, 34517, Egypt.*

[†]These authors contributed equally to this work.

*E-mail: stacey.wetmore@uleth.ca. Tel.: (403) 329-2323.

Contents

Figure S1: Overlay of the active site of ICs obtained from IRCs corresponding to TS1 (IC) and TS2 (IC').....	S1
Figure S2. Active site hydrogen-bond distances (Å) and angles (deg.) for the APE1-catalyzed phosphodiester bond cleavage facilitated by Mg ²⁺ , Mn ²⁺ , Ni ²⁺ (octahedral coordination), or Zn ²⁺	S2
Figure S3. Metal coordination distances (Å) for the APE1-catalyzed phosphodiester bond cleavage facilitated by Mg ²⁺ , Mn ²⁺ , or Ni ²⁺ (octahedral coordination)	S3
Figure S4. Overlay of the active site from a) QM/MM Mg ²⁺ -RC and the crystal structure of Mn ²⁺ containing thio-substituted reactant analogue complex, b) QM/MM Mg ²⁺ -PC and the crystal structure of Mg ²⁺ containing product complex, and c) QM/MM Mn ²⁺ -RC and the crystal structure of Mn ²⁺ containing thio-substituted reactant analogue complex	S4
Figure S5. Overlay of the active site for each stationary point along the APE1-catalyzed phosphodiester bond cleavage facilitated by Mg ²⁺ with respect to the RC	S5
Figure S6. Overlay of the active site for each stationary point along the APE1-catalyzed phosphodiester bond cleavage facilitated by Mn ²⁺ with respect to the corresponding Mg ²⁺ containing structure.....	S6
Figure S7. Metal coordination distances (Å) for the APE1-catalyzed phosphodiester bond cleavage facilitated by square-planar Ni ²⁺	S7

Figure S8. Overlay of the active site for each stationary point along the APE1-catalyzed phosphodiester bond cleavage facilitated by square-planar Ni ²⁺ with respect to the corresponding Mg ²⁺ containing structure	S8
Figure S9. Active site hydrogen-bond distances (Å) and angles (deg.) for the APE1-catalyzed phosphodiester bond cleavage facilitated by square-planar Ni ²⁺	S9
Figure S10. Mechanism and key calculated bond distances (Å) for the APE1-catalyzed phosphodiester bond cleavage facilitated by square-planar Ni ²⁺	S10
Figure S11. Overlay of the active site for each stationary point along the APE1-catalyzed phosphodiester bond cleavage facilitated by octahedral Ni ²⁺ with respect to the corresponding Mg ²⁺ containing structure	S11
Figure S12. Overlay of the active site for each stationary point along the APE1-catalyzed phosphodiester bond cleavage facilitated by Zn ²⁺ with respect to the corresponding Mg ²⁺ containing structure	S12
Figure S13. Metal coordination distances (Å) for the APE1-catalyzed phosphodiester bond cleavage facilitated by Zn ²⁺	S13
Figure S14. Overlay of the active site for each stationary point along the APE1-catalyzed phosphodiester bond cleavage inhibited by Ca ²⁺ with respect to the corresponding Mg ²⁺ containing structure.....	S14
Figure S15. Metal coordination distances (Å) for the APE1-catalyzed phosphodiester bond cleavage inhibited by Ca ²⁺	S15
Figure S16. Overlay of the active site for each stationary point along the APE1-catalyzed phosphodiester bond cleavage inhibited by Ca ²⁺ with respect to the RC	S16
Figure S17. Overlay of the active site for the QM/MM Ca ²⁺ -PC (blue) and the crystal structure of the Mg ²⁺ containing product complex	S17
Table S1: Protonation states of titratable amino acid residues.....	S18
Table S2. Relative energy (kJ/mol) for the APE1-catalyzed phosphodiester bond cleavage facilitated by different metals from the potential energy surface.....	S18
Table S3. Relative Gibbs energy (kJ/mol) for the APE1-catalyzed phosphodiester bond cleavage facilitated by different metals	S19
Table S4: Calculated charge-to-size ratios of different metals in the APE1 reactant complex.....	S19

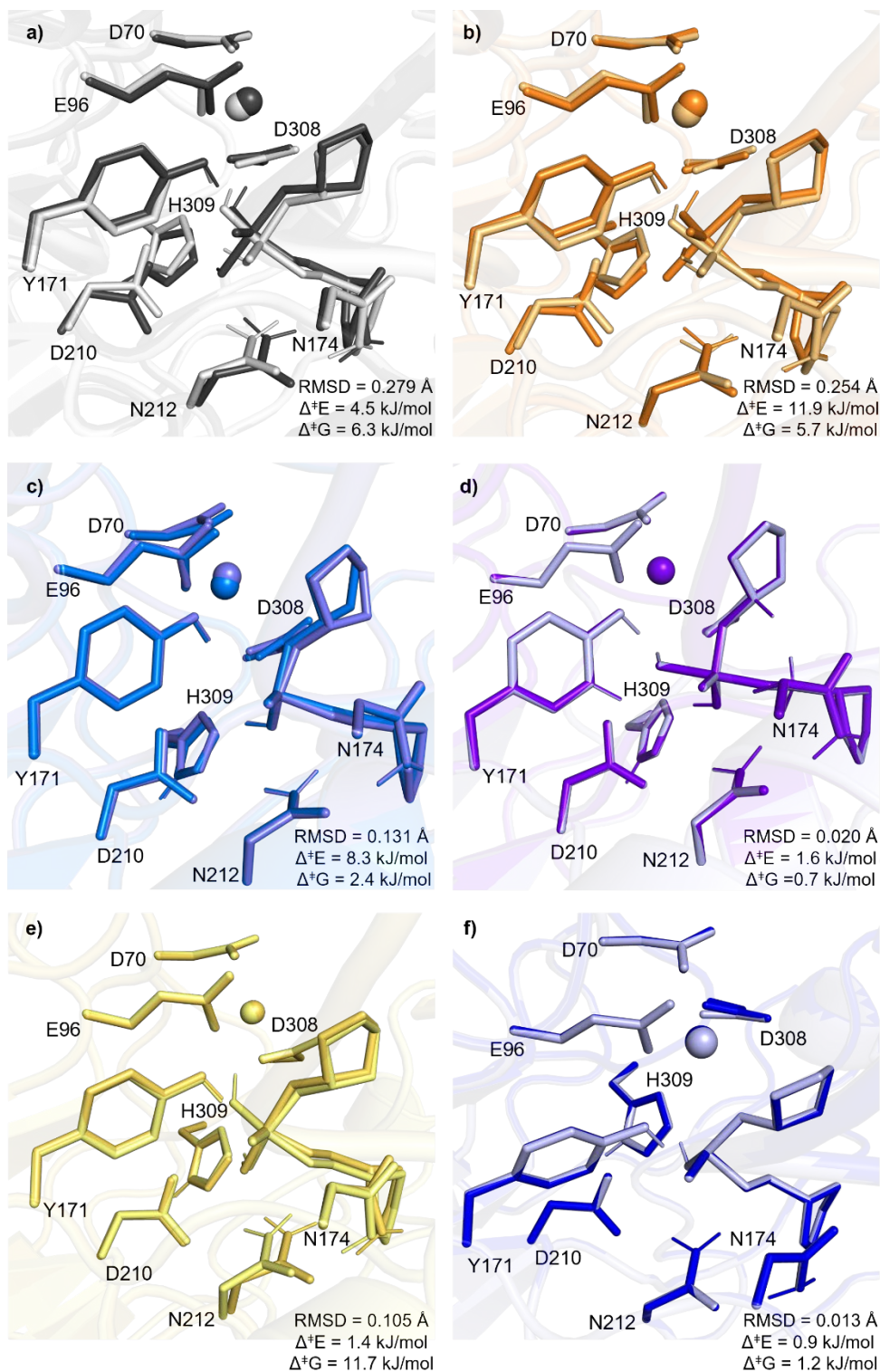


Figure S1: Overlay of the active site of ICs obtained from IRCs corresponding to TS1 (IC) and TS2 (IC') for the APE1-catalyzed phosphodiester bond cleavage facilitated by a) Mg^{2+} , b) Mn^{2+} , c) octahedral Ni^{2+} , d) square-planar Ni^{2+} , e) Zn^{2+} , and f) Ca^{2+} . The energy differences were calculated for IC' with respect to IC.

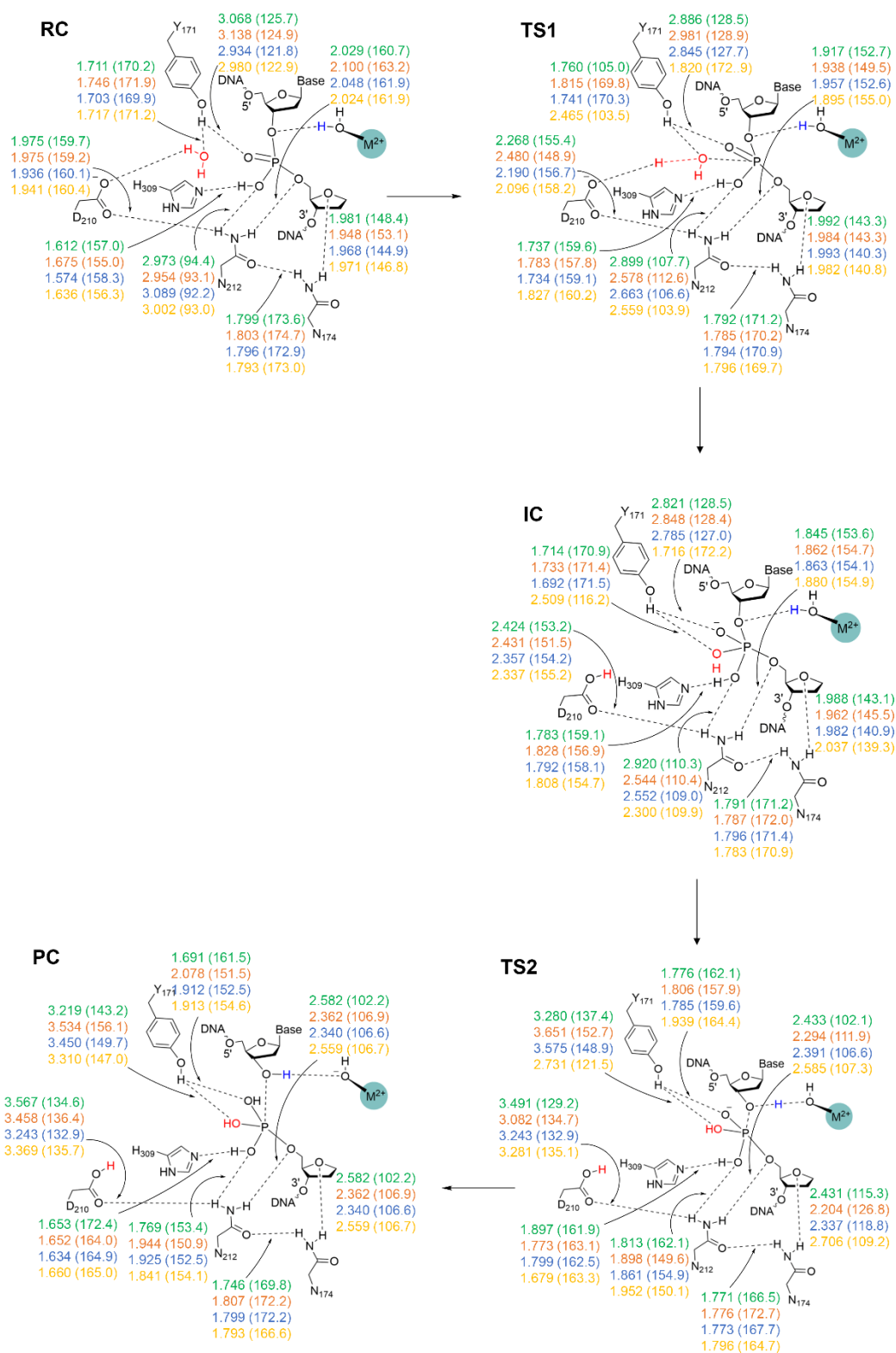


Figure S2: Active site hydrogen-bond distances (Å) and angles (deg., in parentheses) for the APE1-catalyzed phosphodiester bond cleavage facilitated by Mg²⁺ (green), Mn²⁺ (orange), Ni²⁺ (octahedral coordination, blue), or Zn²⁺ (yellow).

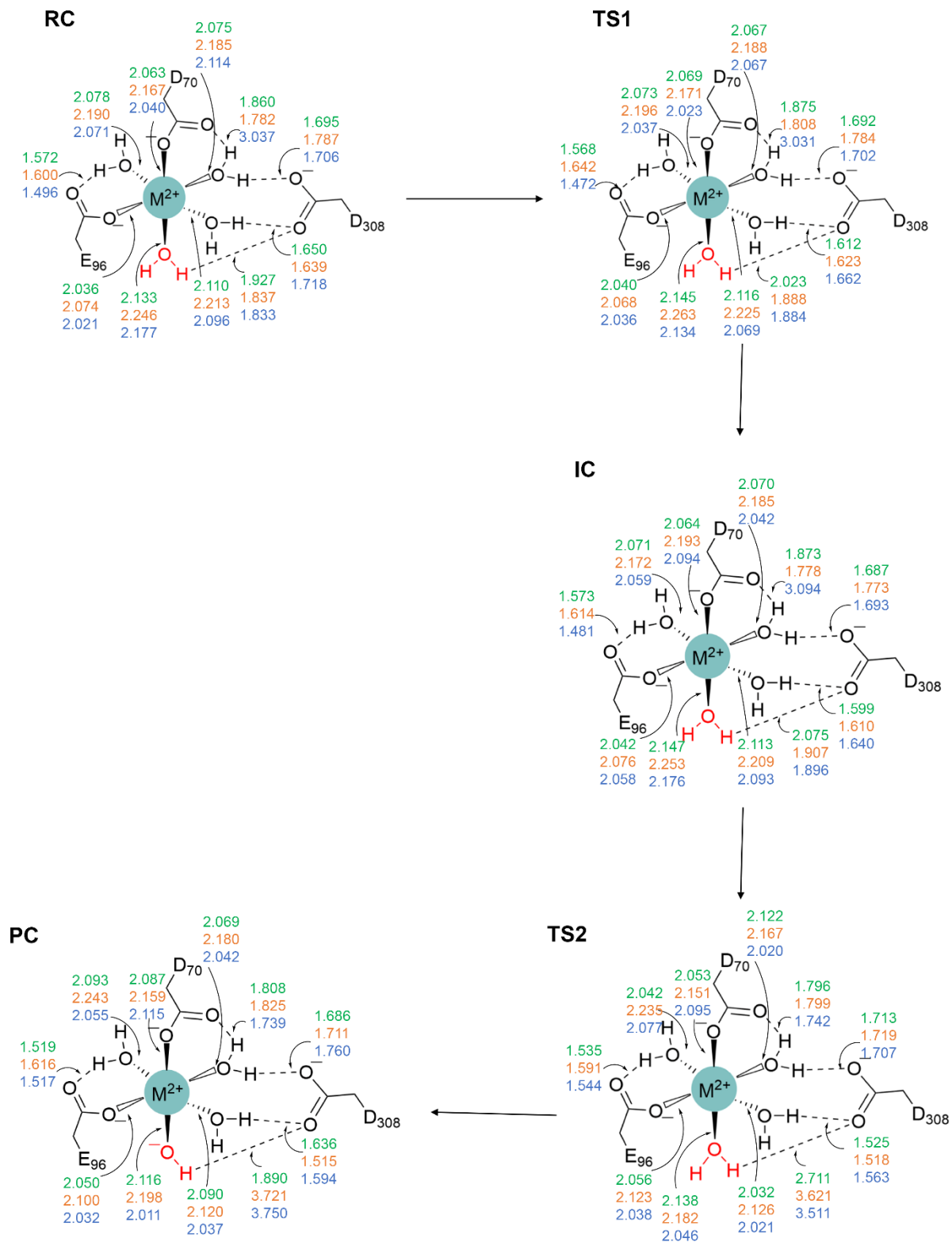


Figure S3: Metal coordination distances (Å) for the APE1-catalyzed phosphodiester bond cleavage facilitated by Mg^{2+} (green), Mn^{2+} (orange), or Ni^{2+} (octahedral coordination, blue). Leaving group protonating water is shown in red.

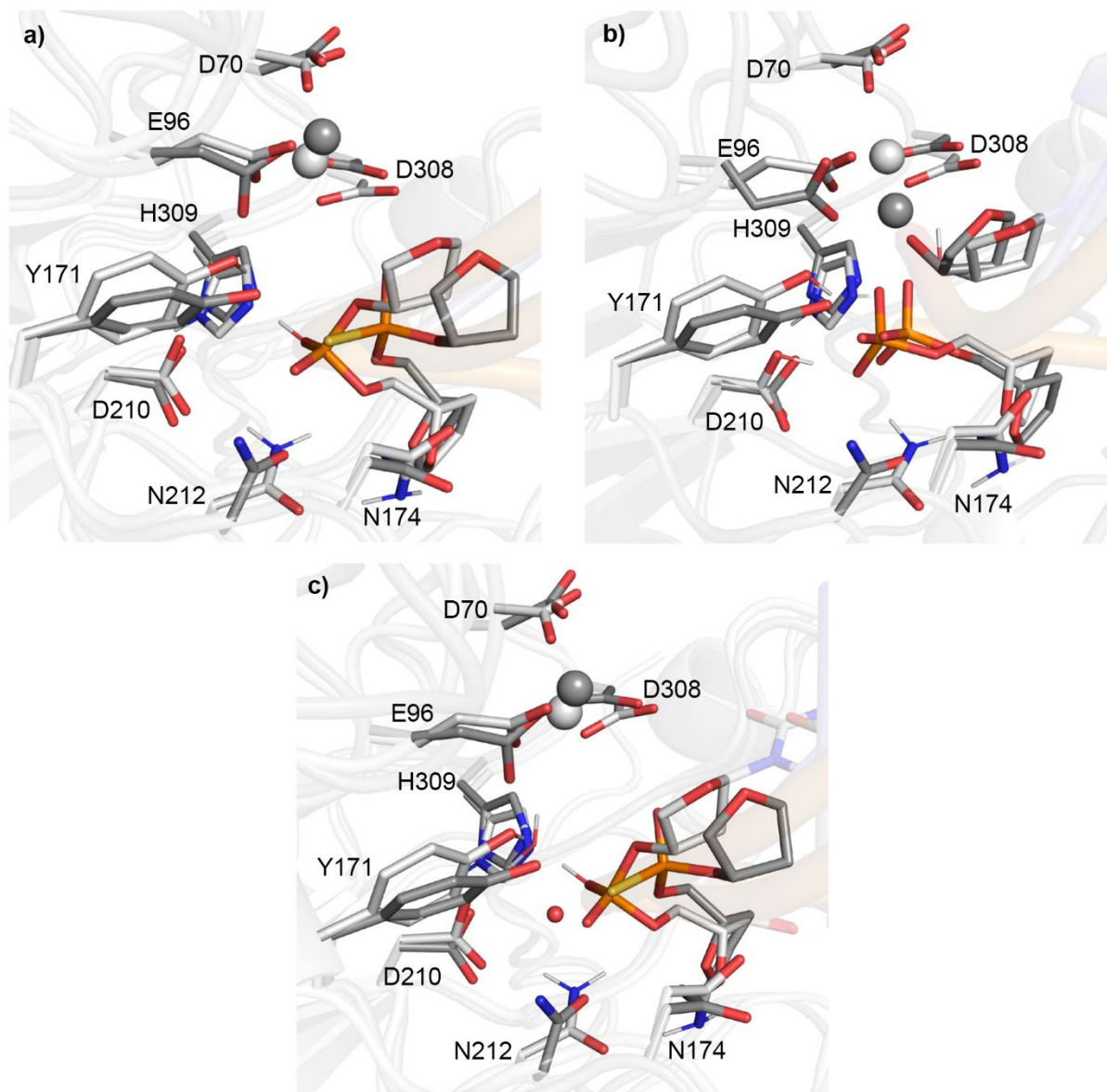


Figure S4: Overlay of the active site from a) QM/MM Mg^{2+} -RC (light grey) and the crystal structure of Mn^{2+} containing thio-substituted reactant analogue complex (dark grey; PDB ID: 5DG0; RMSD = 0.990 Å), b) QM/MM Mg^{2+} -PC (light grey) and the crystal structure of Mg^{2+} containing product complex (dark grey; PDB ID: 4IEM; RMSD = 0.894 Å), and c) QM/MM Mn^{2+} -RC (light grey) and the crystal structure of Mn^{2+} containing thio-substituted reactant analogue complex (dark grey; PDB ID: 5DG0; RMSD = 0.943 Å).

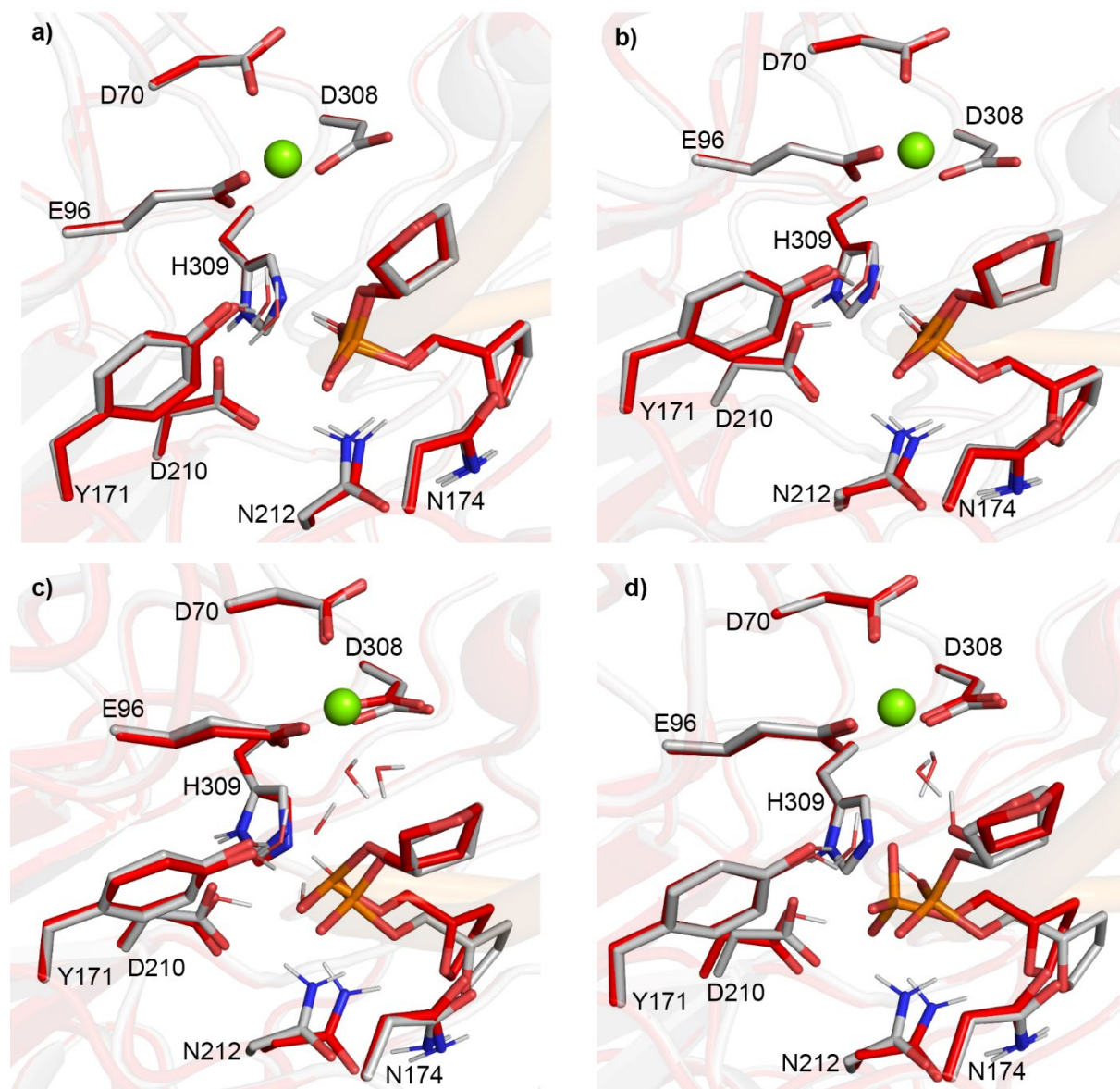


Figure S5: Overlay of the active site for each stationary point along the APE1-catalyzed phosphodiester bond cleavage facilitated by Mg^{2+} (red) with respect to the RC (grey): a) $\text{Mg}^{2+}\text{-RC:Mg}^{2+}\text{-TS1}$ (RMSD = 0.138 Å), b) $\text{Mg}^{2+}\text{-RC:Mg}^{2+}\text{-IC}$ (RMSD = 0.143 Å), c) $\text{Mg}^{2+}\text{-RC:Mg}^{2+}\text{-TS2}$ (RMSD = 0.269 Å), and d) $\text{Mg}^{2+}\text{-RC:Mg}^{2+}\text{-PC}$ (RMSD = 0.321 Å).

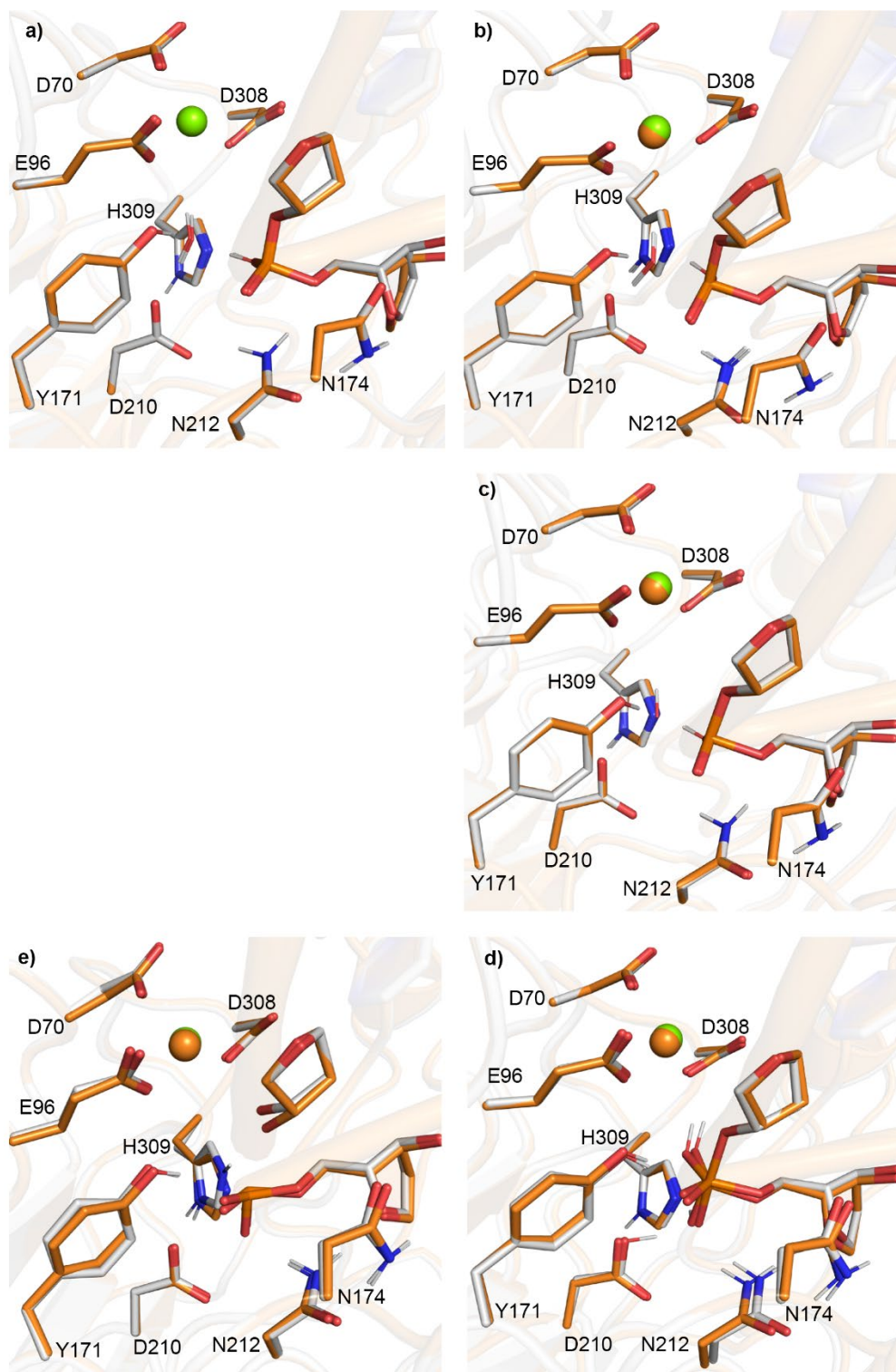


Figure S6: Overlay of the active site for each stationary point along the APE1-catalyzed phosphodiester bond cleavage facilitated by Mn^{2+} (orange) with respect to the corresponding Mg^{2+} containing structure (grey): a) $\text{Mg}^{2+}\text{-RC}:\text{Mn}^{2+}\text{-RC}$ (RMSD = 0.089 Å), b) $\text{Mg}^{2+}\text{-TS1}:\text{Mn}^{2+}\text{-TS1}$ (RMSD = 0.093 Å), c) $\text{Mg}^{2+}\text{-IC}:\text{Mn}^{2+}\text{-IC}$ (RMSD = 0.093 Å), d) $\text{Mg}^{2+}\text{-TS2}:\text{Mn}^{2+}\text{-TS2}$ (RMSD = 0.195 Å), and e) $\text{Mg}^{2+}\text{-PC}:\text{Mn}^{2+}\text{-PC}$ (RMSD = 0.183 Å).

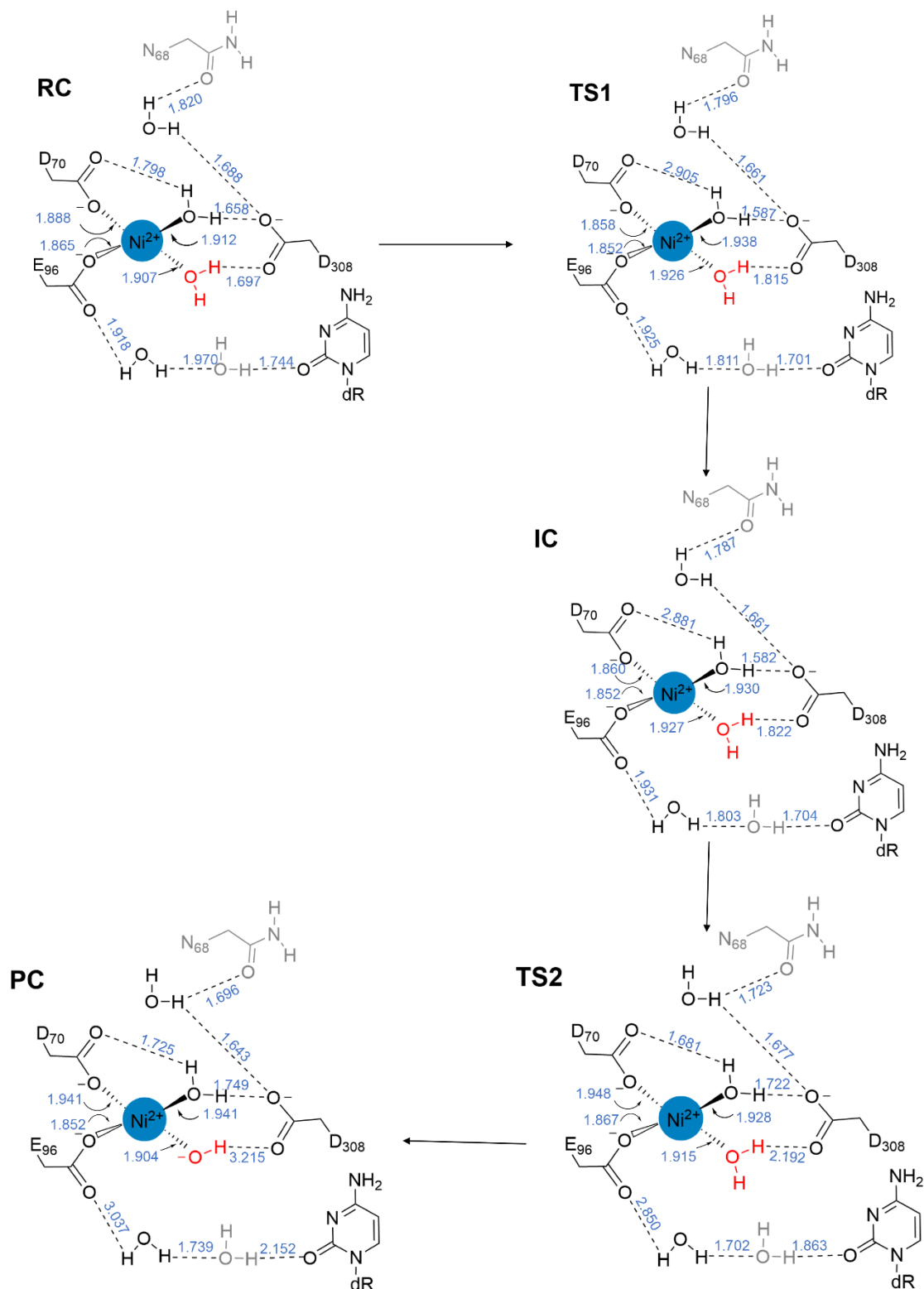


Figure S7: Metal coordination distances (Å) for the APE1-catalyzed phosphodiester bond cleavage facilitated by square-planar Ni^{2+} . Low layer residues are shown in grey and leaving group protonating water in red.

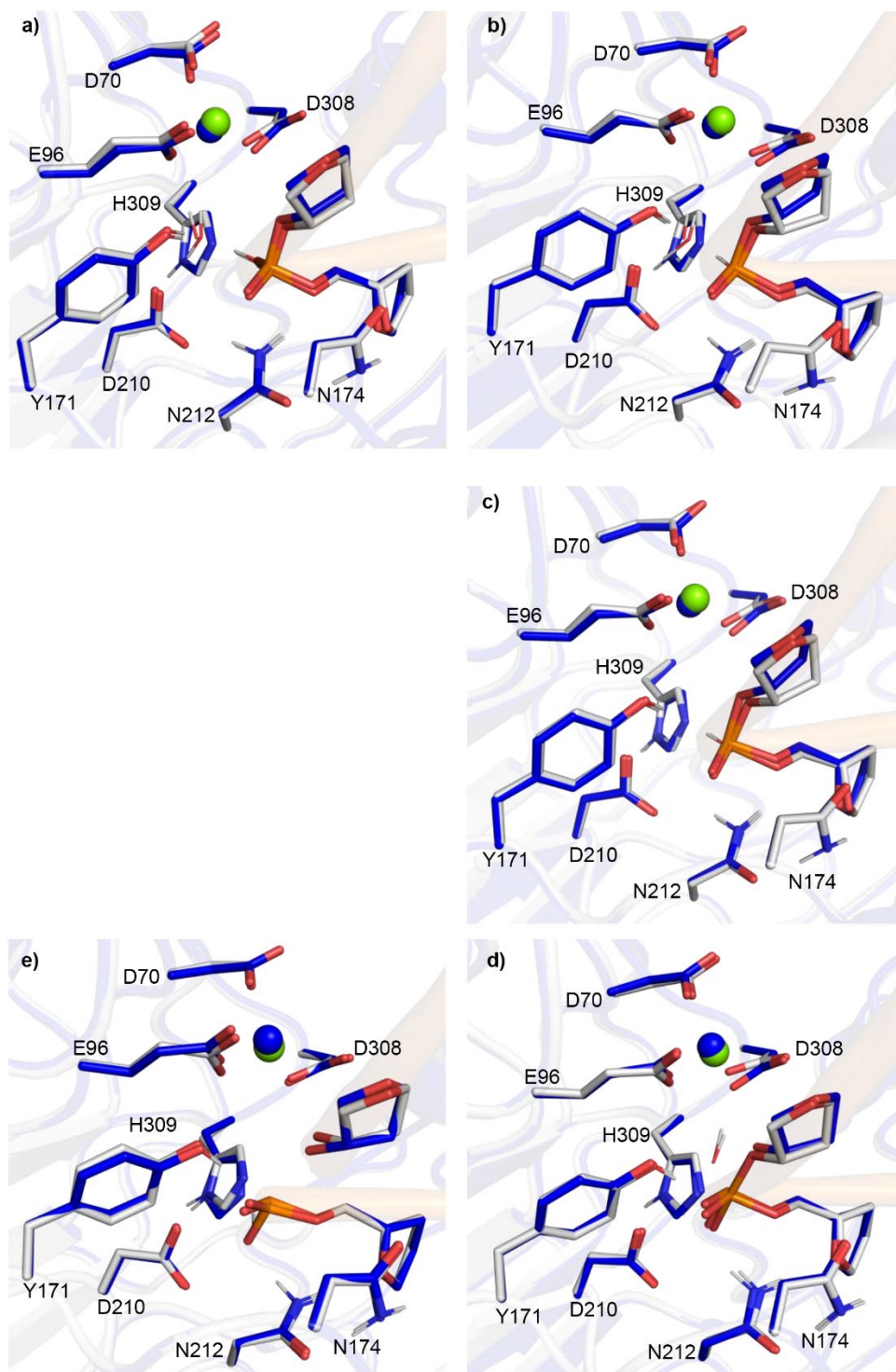


Figure S8: Overlay of the active site for each stationary point along the APE1-catalyzed phosphodiester bond cleavage facilitated by square-planar Ni^{2+} (blue) with respect to the corresponding Mg^{2+} containing structure (grey): a) $\text{Mg}^{2+}\text{-RC}:\text{Ni}^{2+}\text{-RC}$ (RMSD = 0.222 Å), b) $\text{Mg}^{2+}\text{-TS1}:\text{Ni}^{2+}\text{-TS1}$ (RMSD = 0.244 Å), c) $\text{Mg}^{2+}\text{-IC}:\text{Ni}^{2+}\text{-IC}$ (RMSD = 0.246 Å), d) $\text{Mg}^{2+}\text{-TS2}:\text{Ni}^{2+}\text{-TS2}$ (RMSD = 0.227 Å), and e) $\text{Mg}^{2+}\text{-PC}:\text{Ni}^{2+}\text{-PC}$ (RMSD = 0.289 Å).

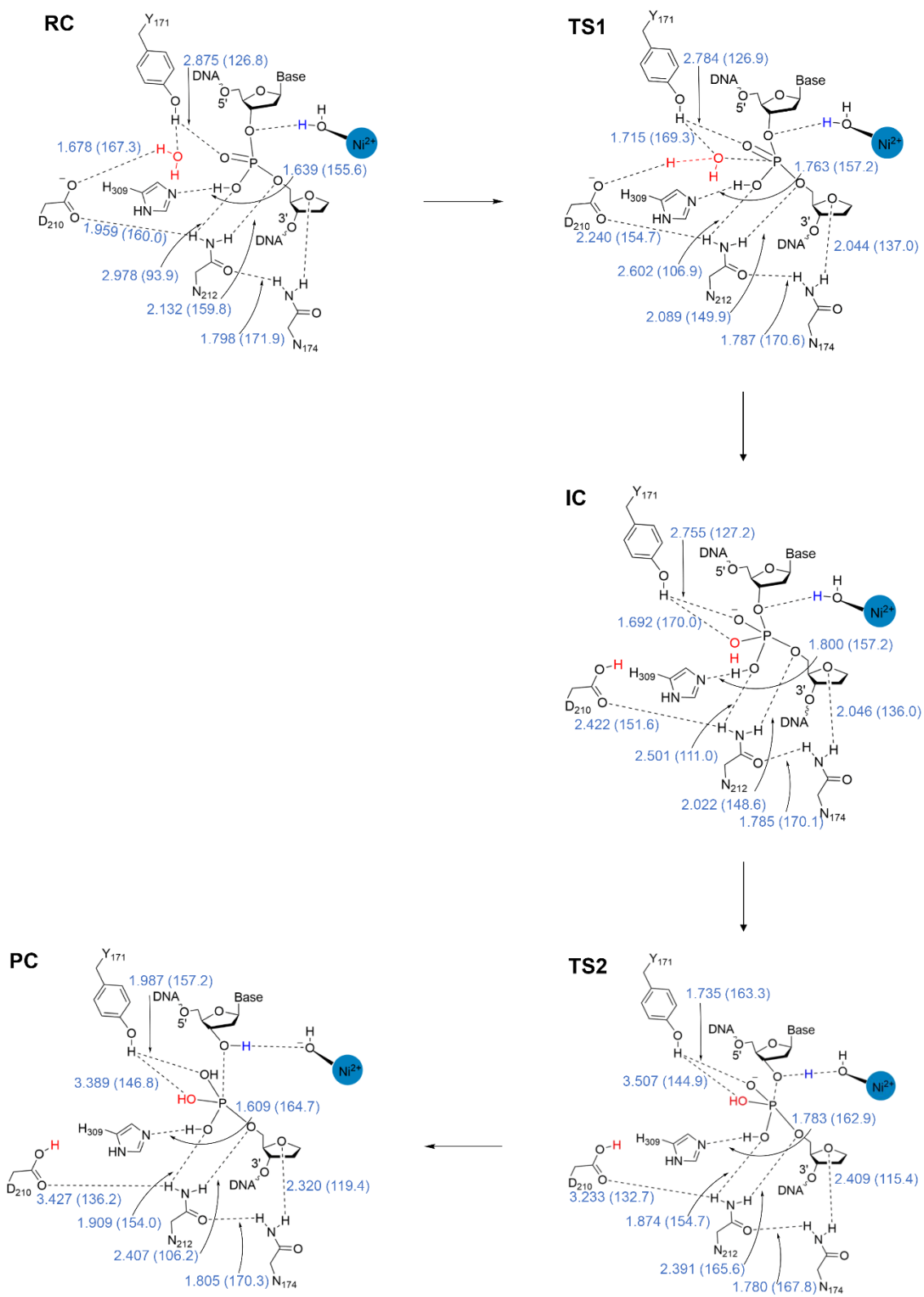


Figure S9: Active site hydrogen-bond distances (Å) and angles (deg., in parentheses) for the APE1-catalyzed phosphodiester bond cleavage facilitated by square-planar Ni²⁺.

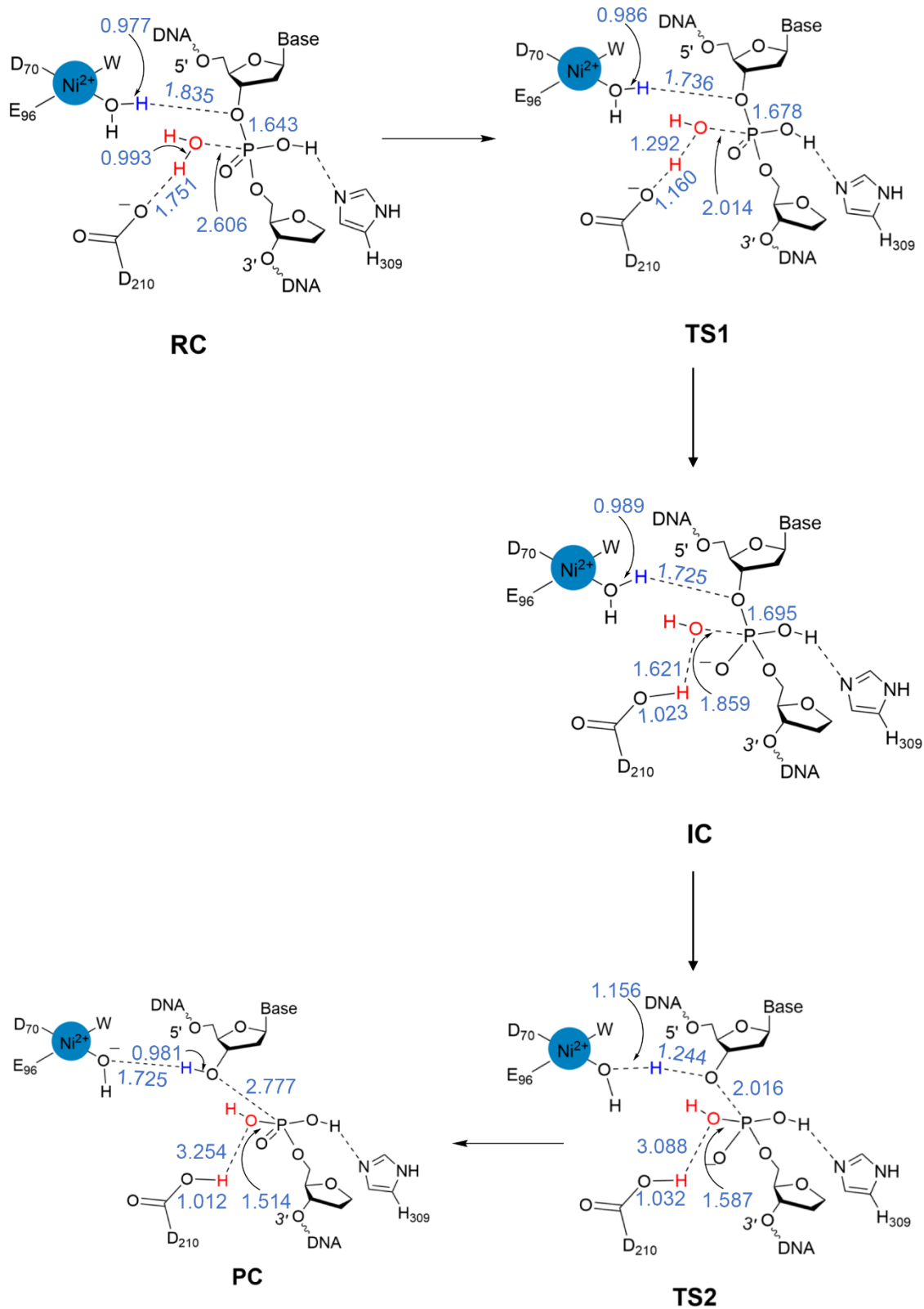


Figure S10: Mechanism and key calculated bond distances (Å) for the APE1-catalyzed phosphodiester bond cleavage facilitated by square-planar Ni²⁺.

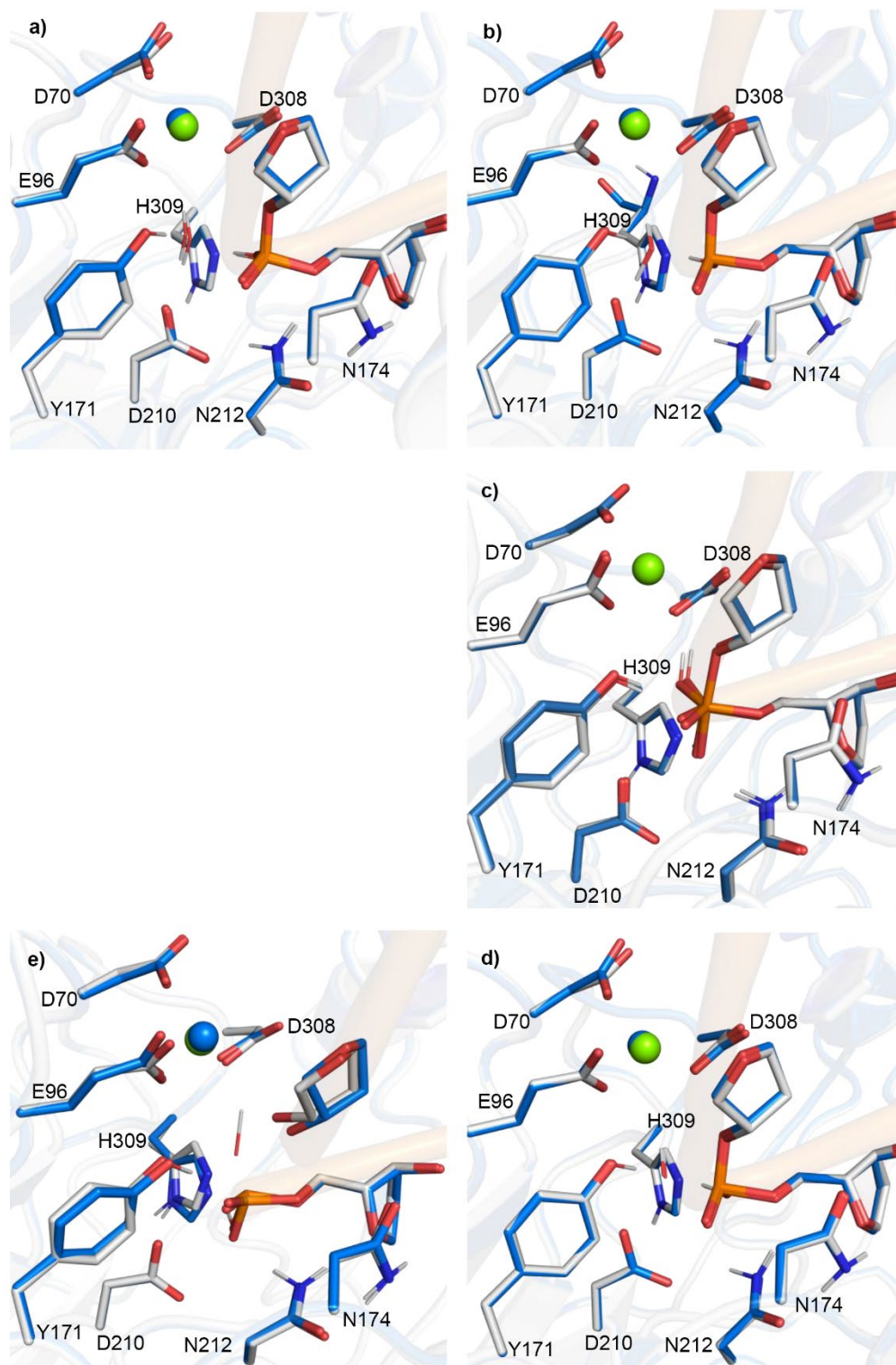


Figure S11: Overlay of the active site for each stationary point along the APE1-catalyzed phosphodiester bond cleavage facilitated by octahedral Ni²⁺ (blue) with respect to the corresponding Mg²⁺ containing structure (grey): a) Mg²⁺-RC:Ni²⁺-RC (RMSD = 0.110 Å), b) Mg²⁺-TS1:Ni²⁺-TS1 (RMSD = 0.083 Å), c) Mg²⁺-IC:Ni²⁺-IC (RMSD = 0.124 Å), d) Mg²⁺-TS2:Ni²⁺-TS2 (RMSD = 0.117 Å), and e) Mg²⁺-PC:Ni²⁺-PC (RMSD = 0.211 Å).

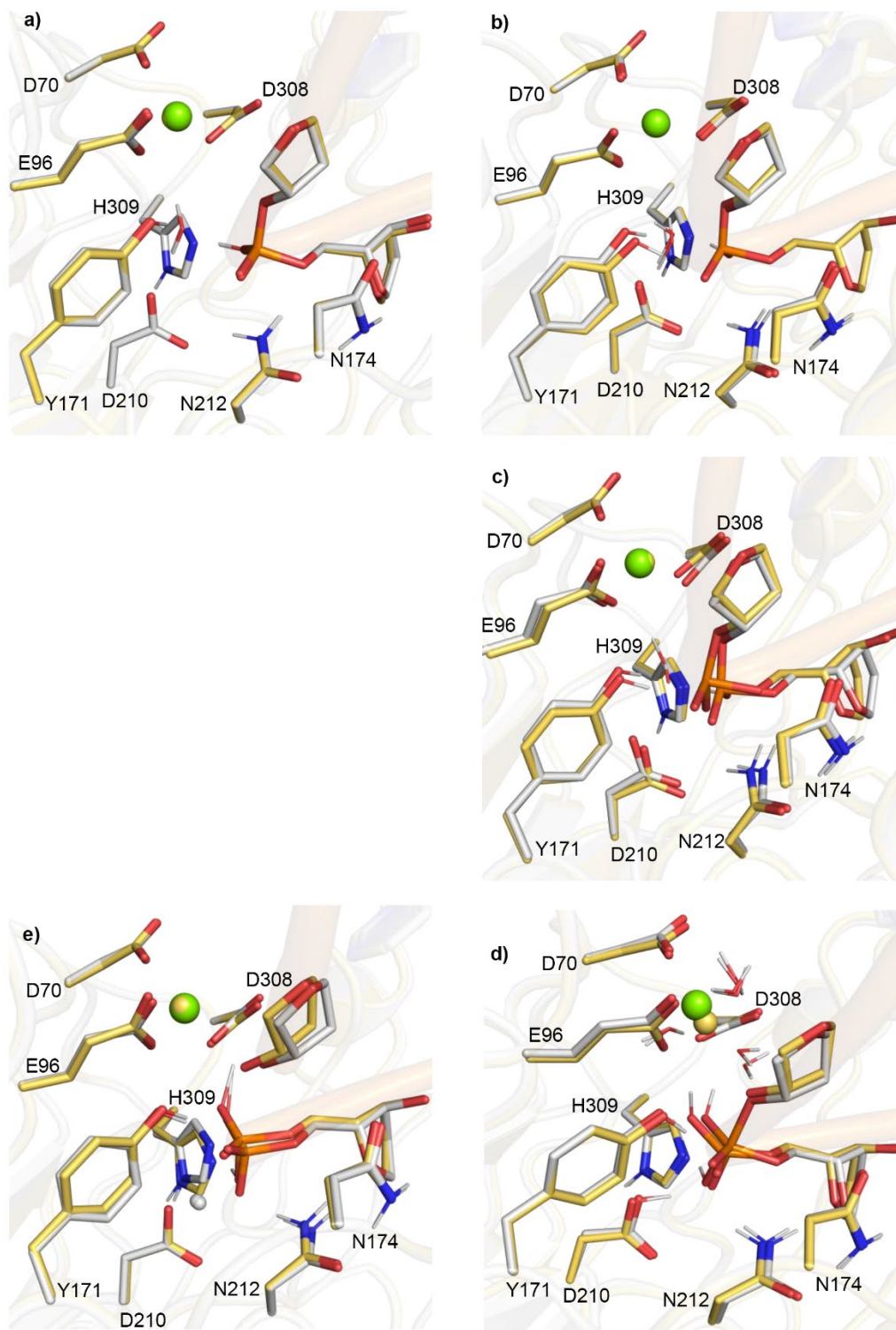


Figure S12: Overlay of the active site for each stationary point along the APE1-catalyzed phosphodiester bond cleavage facilitated by Zn²⁺ (yellow) with respect to the corresponding Mg²⁺ containing structure (grey): a) Mg²⁺-RC:Zn²⁺-RC (RMSD = 0.060 Å), b) Mg²⁺-TS1:Zn²⁺-TS1 (RMSD = 0.144 Å), c) Mg²⁺-IC:Zn²⁺-IC (RMSD = 0.269 Å), d) Mg²⁺-TS2:Zn²⁺-TS2 (RMSD = 0.212 Å) and e) Mg²⁺-PC:Zn²⁺-PC (RMSD = 0.199 Å).

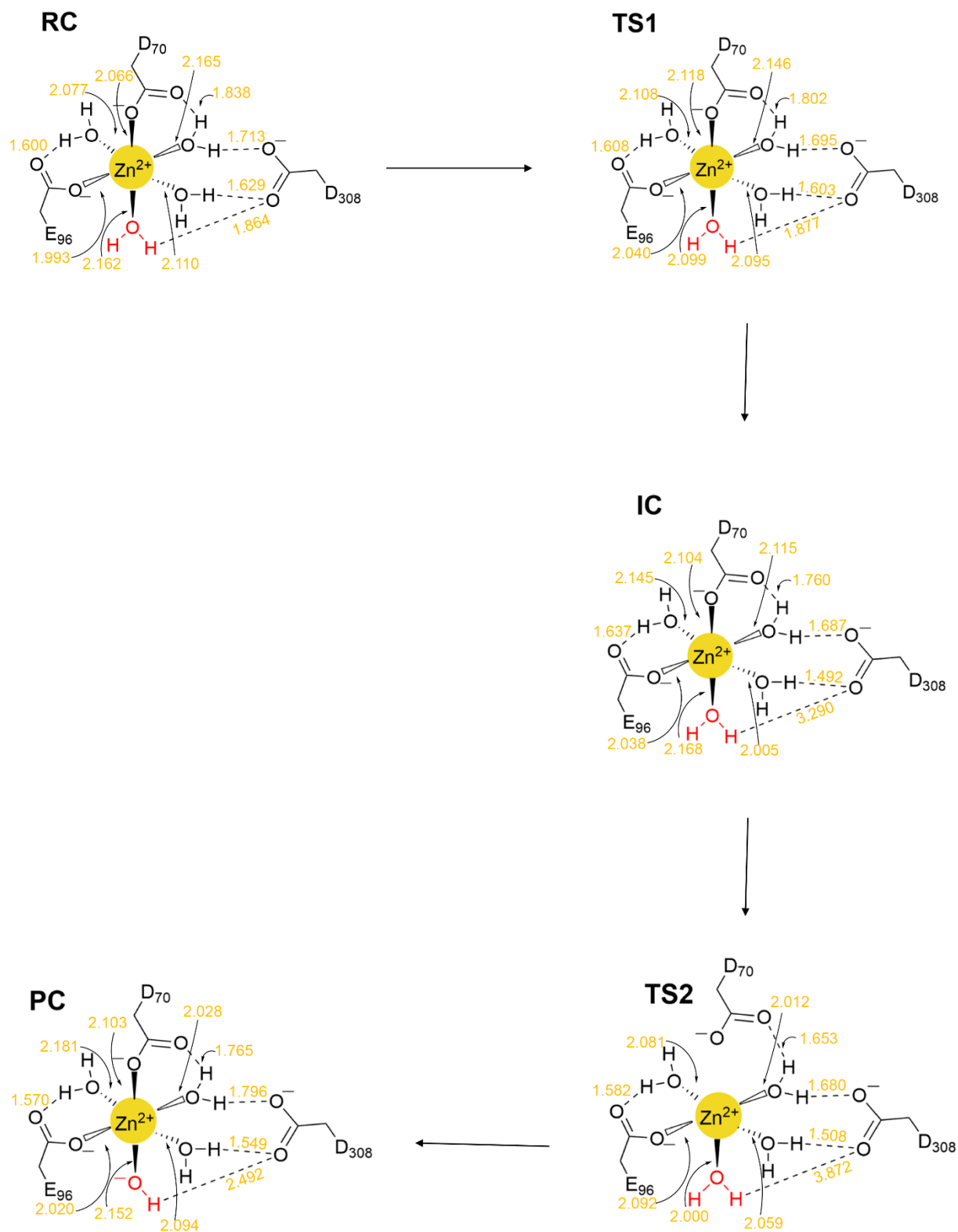


Figure S13: Metal coordination distances (Å) for the APE1-catalyzed phosphodiester bond cleavage facilitated by Zn²⁺. Leaving group protonating water is shown in red.

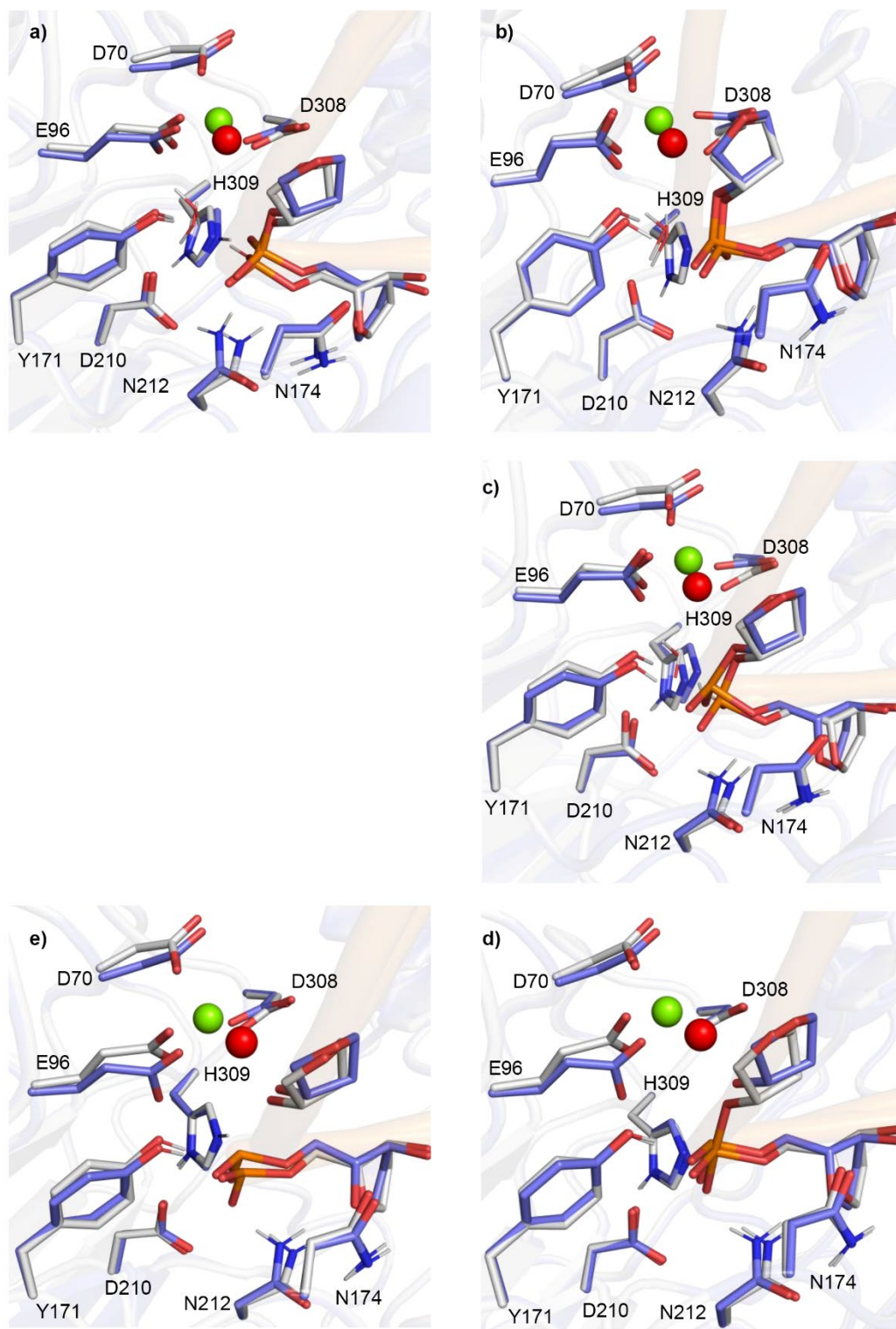


Figure S14: Overlay of the active site for each stationary point along the APE1-catalyzed phosphodiester bond cleavage inhibited by Ca^{2+} (blue) with respect to the corresponding Mg^{2+} containing structure (grey): a) $\text{Mg}^{2+}\text{-RC}:\text{Ca}^{2+}\text{-RC}$ (RMSD = 0.383 Å), b) $\text{Mg}^{2+}\text{-TS1}:\text{Ca}^{2+}\text{-TS1}$ (RMSD = 0.191 Å), c) $\text{Mg}^{2+}\text{-IC}:\text{Ca}^{2+}\text{-IC}$ (RMSD = 0.347 Å), d) $\text{Mg}^{2+}\text{-TS2}:\text{Ca}^{2+}\text{-TS2}$ (RMSD = 0.170 Å), and e) $\text{Mg}^{2+}\text{-PC}:\text{Ca}^{2+}\text{-PC}$ (RMSD = 0.331 Å).

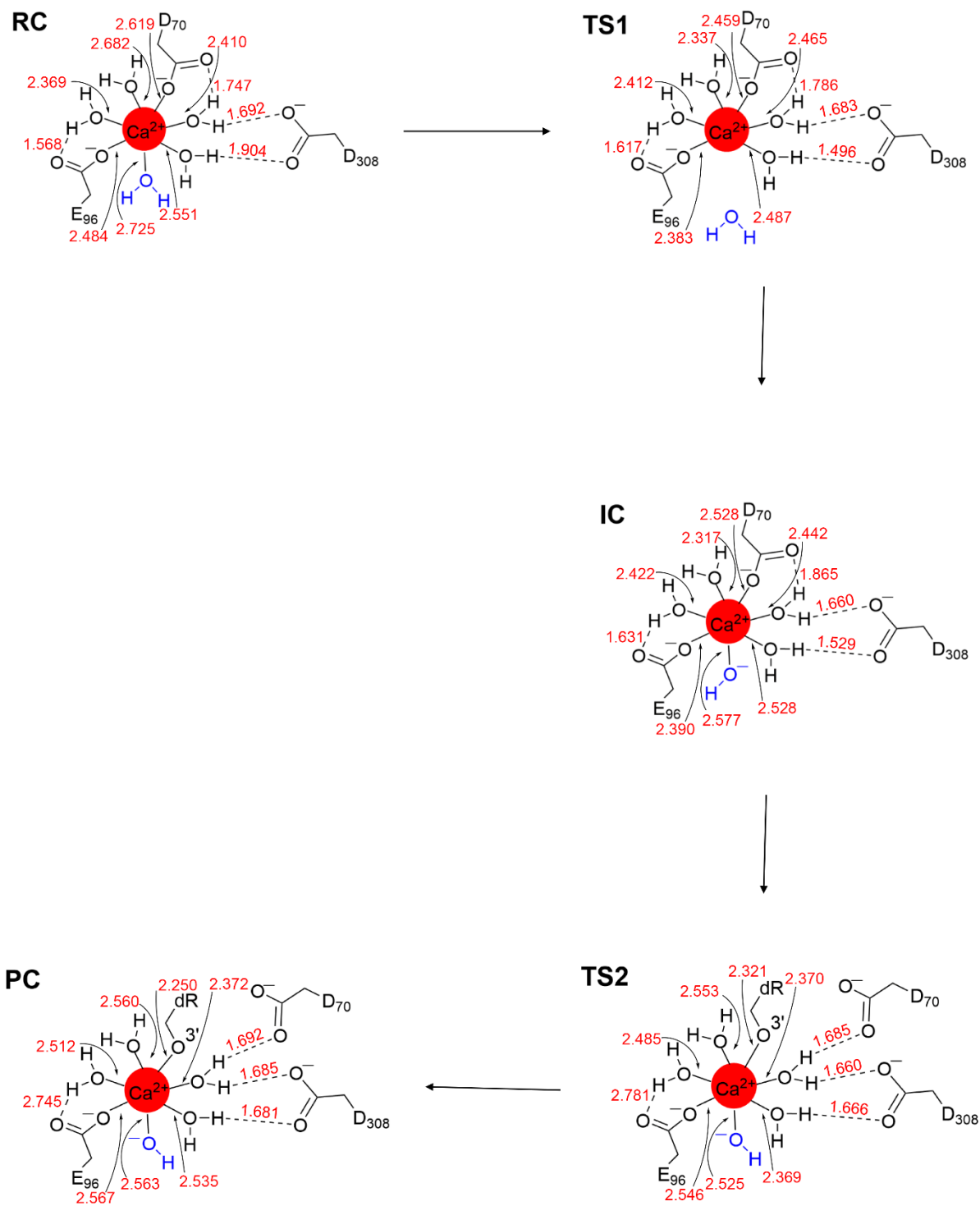


Figure S15: Metal coordination distances (Å) for the APE1-catalyzed phosphodiester bond cleavage inhibited by Ca^{2+} . Nucleophilic water is shown in blue.

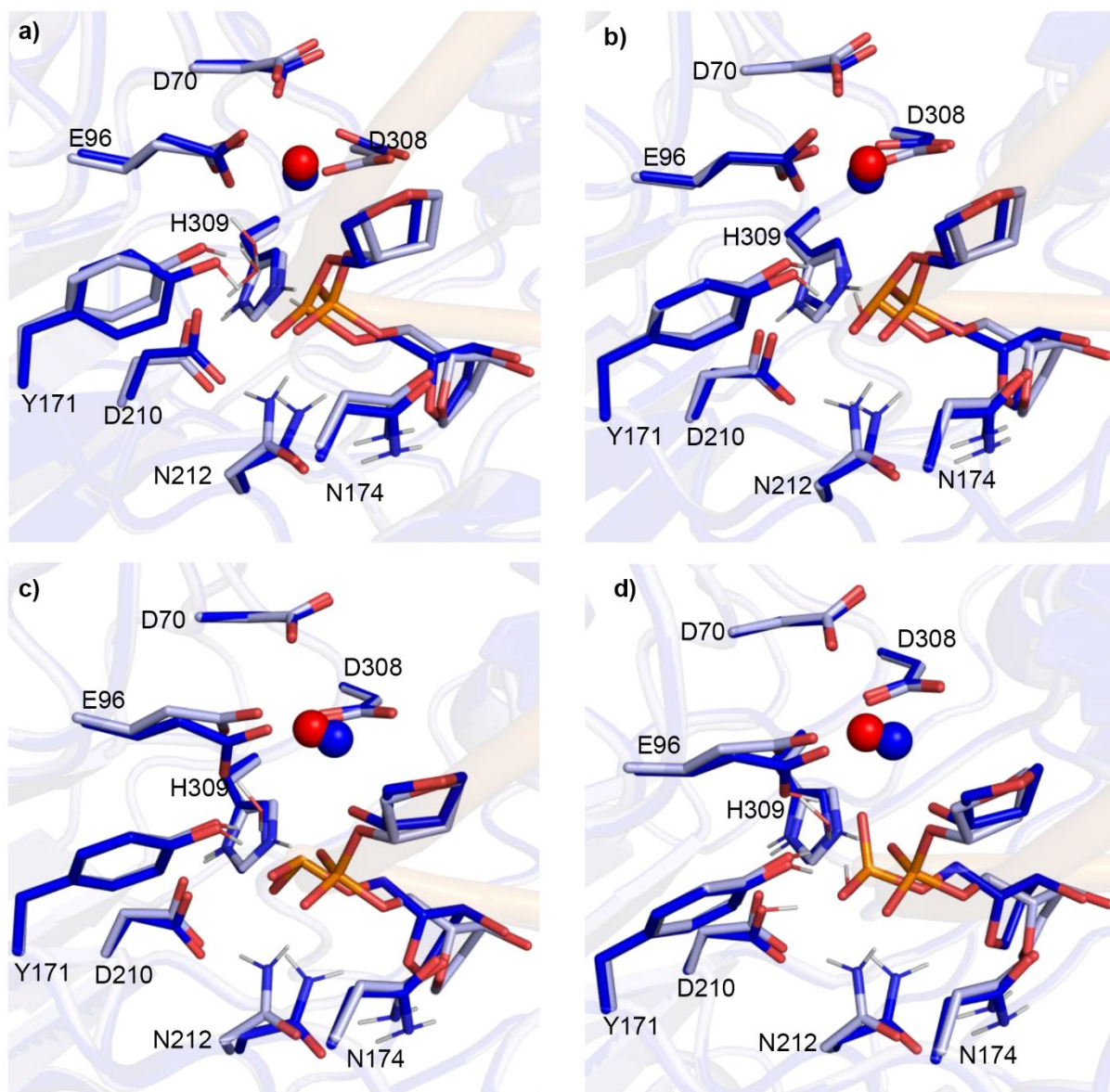


Figure S16: Overlay of the active site for each stationary point along the APE1-catalyzed phosphodiester bond cleavage inhibited by Ca^{2+} (dark blue) with respect to the RC (light blue): a) $\text{Ca}^{2+}\text{-RC}:\text{Ca}^{2+}\text{-TS1}$ (RMSD = 0.455 Å), b) $\text{Ca}^{2+}\text{-RC}:\text{Ca}^{2+}\text{-IC}$ (RMSD = 0.346 Å), c) $\text{Ca}^{2+}\text{-RC}:\text{Ca}^{2+}\text{-TS2}$ (RMSD = 0.192 Å), and d) $\text{Ca}^{2+}\text{-RC}:\text{Ca}^{2+}\text{-PC}$ (RMSD = 0.288 Å).

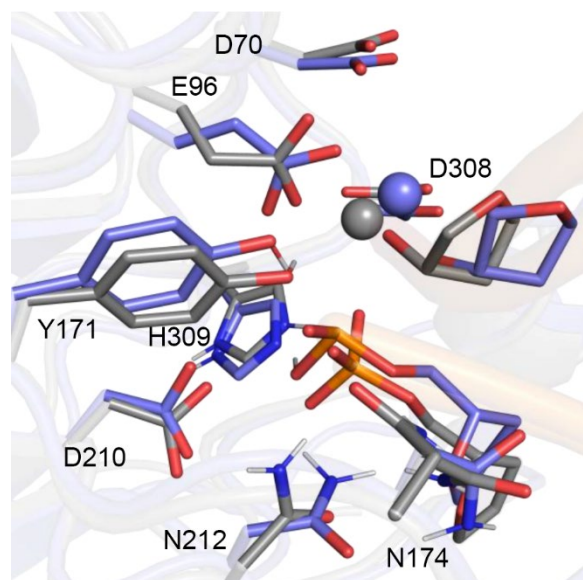


Figure S17: Overlay of the active site for the QM/MM Ca²⁺-PC (blue) and the crystal structure of the Mg²⁺ containing product complex (dark grey; PDB ID: 4IEM; RMSD = 0.842 Å).

Table S1: Protonation states of titratable amino acid residues. ^a

Amino Acid	p <i>K</i> _a	Amino Acid	p <i>K</i> _a	Amino Acid	p <i>K</i> _a
D47	5.23	E217	4.28	K77	10.54
D50	1.57	E236	4.90	K78	11.01
D70	7.18	E242	4.58	K79	10.61
D82	3.70	H116	6.55	K85	10.67
D90	3.99	H151	5.97	K98	12.62
D124	3.75	H215	5.55	K103	10.44
D148	3.74	H255	5.79	K125	10.66
D152	4.16	H289	6.02	K141	10.55
D163	3.69	H309	10.35	K194	10.80
D189	5.57	C65	12.59	K197	10.22
D210	7.54	C93	17.79	K203	10.90
D219	2.28	C99	10.49	K224	10.45
D251	4.39	C138	8.98	K227	10.05
D283	4.45	C208	8.17	K228	11.28
D297	3.63	C296	10.66	K276	11.36
D308	3.85	C310	12.74	K299	10.71
E46	4.43	Y45	14.32	K303	10.56
E86	4.66	Y118	12.03	R73	12.59
E87	4.76	Y128	13.35	R136	12.81
E96	4.77	Y144	11.27	R156	16.31
E101	5.15	Y171	17.30	R177	9.65
E107	4.39	Y184	12.19	R181	13.55
E110	4.71	Y257	12.81	R185	13.41
E126	4.53	Y262	9.98	R187	13.12
E149	4.67	Y264	12.86	R193	12.42
E150	4.00	Y269	15.89	R202	12.44
E154	4.14	Y284	14.57	R221	12.56
E161	3.91	Y315	12.86	R237	12.33
E183	4.41	K52	10.49	R254	12.14
E190	4.07	K58	10.72	R274	11.63
E216	4.51	K63	9.82		

^aThe physiological protonation states of titratable amino acid residues were verified using the propKa server.

Table S2: Relative energy (kJ/mol) for the APE1-catalyzed phosphodiester bond cleavage facilitated by different metals from the potential energy surface. ^a

Stationary point	Mg ²⁺	Mn ²⁺	Ni ²⁺ (s.p.) ^b	Ni ²⁺ (oct.) ^c	Zn ²⁺	Ca ²⁺
RC	0.0	0.0	0.0	0.0	0.0	0.0
TS1	37.3	44.0	47.0	33.2	64.1	115.2
IC	28.3	35.9	32.4	28.8	38.6	75.5
TS2	42.7	43.1	61.9	102.8	85.5	89.1
PC	-84.9	-18.8	-37.5	8.2	-41.0	4.4

^aRelative energies evaluated with ONIOM(B3LYP-D3(BJ)/6-31G(d,p):AMBER). ^bSquare planar coordination. ^cOctahedral coordination.

Table S3: Relative Gibbs energy (kJ/mol) for the APE1-catalyzed phosphodiester bond cleavage facilitated by different metals.^a

Stationary point	Mg ²⁺	Mn ²⁺	Ni ²⁺ (s.p.) ^b	Ni ²⁺ (oct.) ^c	Zn ²⁺	Ca ²⁺
RC	0.0	0.0	0.0	0.0	0.0	0.0
TS1	64.8	69.8	63.1	74.3	91.1	137.7
IC	60.9	68.2	61.9	70.3	71.8	81.8
TS2	65.1	71.5	74.7	88.8	109.2	100.1
PC	-57.4	-30.3	-35.0	-41.5	-20.9	-11.9

^aRelative energies evaluated with ONIOM(M06-2X/6-311+G(2df,p):AMBER)+ Δ_{Gibbs} //ONIOM(B3LYP-D3(BJ)/6-31G(d,p):AMBER). ^bSquare planar coordination. ^cOctahedral coordination.

Table S4: Calculated charge-to-size ratios of different metals in the APE1 reactant complex.

	Mg ²⁺	Mn ²⁺	Ni ²⁺ (s.p.) ^b	Ni ²⁺ (oct.) ^c	Zn ²⁺	Ca ²⁺
Ionic radius of the metal	0.65	0.75	0.72	0.72	0.74	0.99
Charge on the metal ^a	1.697	1.715	0.980	1.102	1.274	1.763
Charge-to-size ratio	2.611	2.287	1.531	1.361	1.722	1.781

^aNBO charges evaluated using B3LYP-D3(BJ)/6-31G(d,p) calculations on a model of the RC that includes only the QM region. Hydrogen atom positions at the truncation points were optimized at the same level of theory while constraining the remainder of the model. ^bSquare planar coordination. ^cOctahedral coordination.